



# Influence of Increased Confining Stress on Undrained Behavior of Tailings: A Case History at the Candelaria Mine

**Peter K. Robertson**, *PK Robertson Inc., Newport Beach, USA; email: [probertson2005@me.com](mailto:probertson2005@me.com)*

**Ken Brouwer**, *Principal Engineer, Knight Piésold Ltd., Vancouver, Canada; email: [kbrouwer@knightpiesold.com](mailto:kbrouwer@knightpiesold.com)*

**Thomas E. Sully**, *Senior Engineer, Knight Piésold Ltd., Vancouver, Canada; email: [tsully@knightpiesold.com](mailto:tsully@knightpiesold.com)*

**Andre Gagnon**, *Director, Tailings & Geotechnical Engineering, Lundin Mining Corporation, Toronto, Canada; email: [andre.gagnon@lundinmining.com](mailto:andre.gagnon@lundinmining.com)*

**ABSTRACT:** Recent failures of mine tailings structures in Brazil have highlighted the importance of the undrained behavior of loose tailings. Loose, saturated tailings can experience significant and rapid strength loss if triggered to behave undrained under shear, and this process has been described as either flow or static liquefaction. A review of case histories has shown that these failures occur at small effective confining stresses, typically less than three atmospheres (300kPa). This observation is also supported by laboratory testing that shows that the Critical State Line (CSL) of these sand-like materials is curved at higher confining stress and that the curvature reduces the brittleness of soils at high confining stresses. The curvature of the CSL is a function of the grain characteristics of the soil. This paper presents an overview of this effect based on published laboratory data on a wide range of soils and outlines a framework to apply this to design. The suggested framework is then compared to data from a case history. The case history involved a thick deposit of loose tailings at the Candelaria Mine where cone penetration testing (CPT) and associated laboratory testing were carried out. Two large test pads were constructed to increase the overburden stress on the tailings, and pre- and post-construction CPT data were collected. The CPT and laboratory data were then compared to the published laboratory data to evaluate the change in undrained behavior with increasing confining stress.

**KEYWORDS:** case history, tailings, undrained strength, effective stress

**SITE LOCATION:** [Geo-Database](#)

## INTRODUCTION

Recent failures of mine tailings structures have highlighted the importance of the undrained behavior of loose tailings. Loose, saturated tailings can experience significant and rapid strength loss if triggered to behave undrained under shear, and this process has been described as either flow or static liquefaction. A flow (static) liquefaction failure is due to a significant and rapid strength loss in undrained shear that can occur in any saturated or near saturated loose soil, such as very loose sands and silts, and it is a major design issue for large soil structures such as mine tailings impoundments and earth dams. For a slope to experience instability due to flow liquefaction, the following conditions are required:

- Loose saturated or near saturated soils that are contractive at large strains and can experience significant and rapid strength loss in undrained shear,
- High static shear stresses (i.e., sloping ground) relative to the resulting large strain undrained shear strength,
- Event(s) that can trigger strength loss,
- Sufficient volume of loose saturated and near saturated soils for instability to manifest, and

Submitted: 25 March 2022; Published: 16 October 2023

Reference: Robertson P. K., Brouwer K., Sully T. E., and Gagnon A. (2023). Influence of Increased Confining Stress on Undrained Behavior of Tailings: A Case History. International Journal of Geoengineering Case Histories, Volume 7, Issue 3, pp. 34-55, doi: 10.4417/IJGCH-07-03-03

- Unsuitable geometry to enable instability.

These conditions were determined to exist at the Stava, Brumadinho, and Fundao mine sites, which experienced flow liquefaction failures (Berti et al., 1997; Robertson et al., 2019; Morgenstern et al., 2016).

The events that can trigger strength loss cover a wide range of conditions, as summarized by Robertson et al. (2019). In general, any form of loading that results in a decrease in mean effective stress has the highest potential to trigger undrained strength loss. Sasitharan et al. (1993) showed that slow drained loading could trigger undrained strength loss when the mean effective stress is reduced. Experience has also shown that the trigger events can be very small (Robertson et al., 2019). If a soil can strain soften in undrained shear and hence is susceptible to flow liquefaction, an estimate of the resulting large strain liquefied shear strength is required for stability analyses. Several recent failures of mine tailings have shown that when significant and rapid strength loss occurs in critical sections of a soil structure, the resulting failures are often very fast, occur with little warning, and the resulting deformations are often very large (e.g., Morgenstern et al., 2016, Robertson et al., 2019). Case histories involving flow liquefaction failures also show that the initial effective confining stress prior to strength reduction was less than 300kPa and mostly less than 200kPa (Robertson, 2017). With increasing height of some tailings structures, there is a need for an improved understanding of the undrained behavior of loose mine tailings at high confining stresses.

The objective of this paper is to present published laboratory data on a range of sandy soils to develop a framework on how increased confining stresses influence the large strain undrained strength ratio of soils, and to compare this with data from the Candelaria Mine case history where the overburden stress on shallow loose tailings was increased significantly using two large test pads of waste rock.

## LABORATORY EVIDENCE

Critical State Soil Mechanics (CSSM) provides a powerful framework to evaluate soil behavior and is based on the observation that soils ultimately reach a critical state (CS) at large strain, and at CS there is a unique relationship between shear stress ( $q$ ), mean effective stress ( $p'$ ), and void ratio ( $e$ ) for a given loading direction. Since CS is independent of the initial state, the parameters that define CS depend only on the nature of the grains of the soils and can be linked to basic soil classification and grain characteristics (e.g., Atkinson, 2007). The behavior of soils in shear prior to failure can be classified into two groups: soils that dilate at large strains and soils that contract at large strains. Saturated soils that are loose contract at large strains and have a shear strength in undrained loading that is lower than the strength in drained loading, whereas saturated soils that are dense dilate at large strains and tend to have a shear strength in undrained loading that is either equal to or larger than in drained loading. When saturated soils contract at large strains they may also show a strain softening response in undrained shearing, although not all soils that contract show a strain softening response in undrained shear.

At low confining stress, the CSL for many clean silica-based sands can be very flat in terms of  $e$  versus  $\log p'$ ; however, at high stress, the consolidation lines for sand-like soils tend to converge to a unique Limiting Compression Curve (LCC) that becomes parallel to the CSL (Pestana and Whittle, 1995).

Jefferies and Been (2016) presented a summary of typical CSLs for a wide range of sand-like soils where each CSL was approximated by a straight line over the limited stress range tested ( $p' < 3\text{atm}$ ). There are several examples where the CSL has been determined over a wider stress range (e.g., Vesic and Clough, 1968; Verdugo and Ishihara, 1996; Schnaid et al., 2013). Figure 1 compares the measured CSLs for a range of sand-like soils in terms of relative density ( $D_r$ ) versus  $\log p'$ . Relative density is used to normalize the CSL (Konrad and Watts, 1995). Use of  $D_r$  is approximate, since there can be some uncertainty in the maximum and minimum void ratio ( $e_{\max}$  and  $e_{\min}$ ), but it provides a useful framework to compare data from a wide range of sand-like soils.

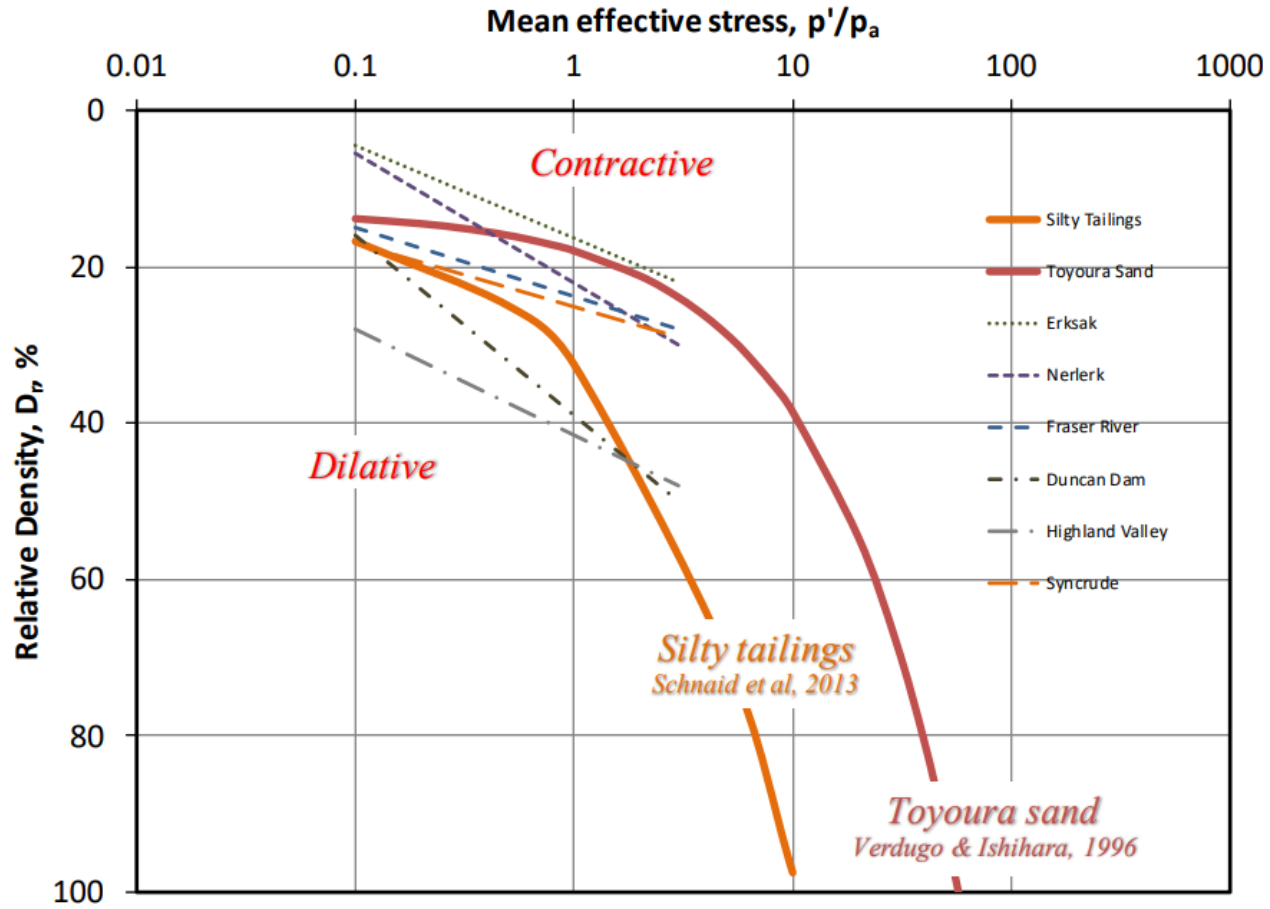


Figure 1. Comparison of published Critical State Lines (CSL) for a wide range of sand-like soils ( $p_a$  = atmospheric pressure  $\sim 100\text{kPa}$ ).

The data on Figure 1 illustrates that the curvature of relatively incompressible clean silica sand, such as Toyoura sand, occurs at higher stresses compared to a more compressible silty sand, such as the silty tailings (Schnaid et al., 2013).

In-situ state can be defined in terms of either state parameter ( $\psi$ ) or a Reference Stress Ratio (RSR), as suggested by Robertson and Fear (1995) and shown on Figure 2. The RSR can be interchanged with  $\psi$ , using:

$$\text{RSR} = p'_o / p'_{cs} = 10^{(\psi/\lambda)} \quad (1)$$

Where  $p'_o$  is the current in-situ mean effective stress,  $p'_{cs}$  is the mean effective stress at CS for the same void ratio, and  $\lambda$  is the slope of the CSL over the stress range between  $p'_o$  and  $p'_{cs}$ .

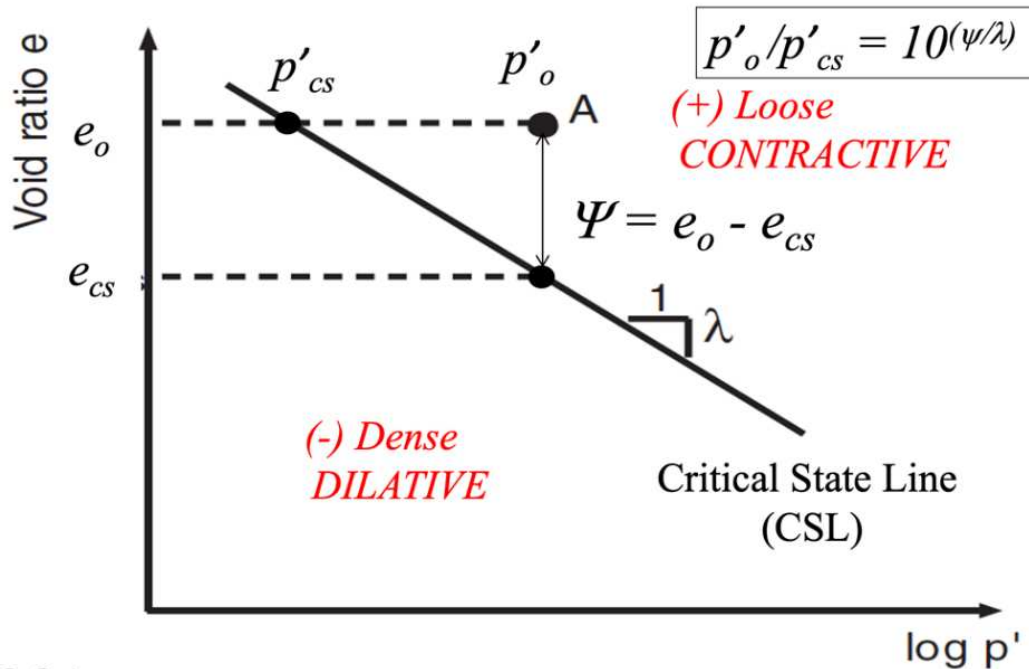


Figure 2. State parameter ( $\psi$ ) and Reference Stress Ratio ( $p'_0/p'_{cs}$ ).

Data from Erksak sand (Jefferies and Been, 2016) can be used to illustrate the influence of increasing confining stress on the undrained behavior of sand-like soils. Erksak sand is a uniform clean silica sub-rounded sand (like Toyoura sand), where the CSL becomes highly non-linear at high stresses and the slope of the CSL line approaches values similar to either compressible sand-like soils (e.g., carbonate sands) or clay-like soils. Jefferies and Been (2016) did sufficient testing on Erksak sand to also define the Limiting Compression Curve (LCC) that is also shown on Figure 3. Figure 3 shows the start and end points for three example isotropically consolidated undrained triaxial compression tests performed on reconstituted samples from very loose states. Full details and associated test results are contained in Jefferies and Been (2016). The slope of the CSL ( $M$ ) at CS for Erksak sand, in triaxial compression, is  $M_{tc} = 1.2$  (i.e.,  $\phi'_{cs} = 30^\circ$ ). For isotropically consolidated undrained triaxial compression tests, the undrained shear strength at CS is  $S_{u(cs)}$  and is assumed, for simplicity, to be  $q_{(cs)}/2$ . Since the slope of the CSL,  $M_{tc}$ , is defined as  $M_{tc} = q_{(cs)}/p'_{(cs)}$ , it follows that:

$$S_{u(cs)} = q_{(cs)}/2 = M_{tc} p'_{cs} / 2 \quad (2)$$

$$S_{u(cs)}/p'₀ = M_{tc} (p'_{cs}/p'₀)/2 \quad (3)$$

For isotropically consolidated triaxial tests  $\sigma'_{vo} = p'₀$ . Hence:

$$S_{u(cs)}/\sigma'_{vo} = (M_{tc}/2) / (p'₀/p'_{cs}) \quad (4)$$

The above simplified relationships agree very well with the test results on Erksak sand (Jefferies and Been, 2016) shown in Table 1.

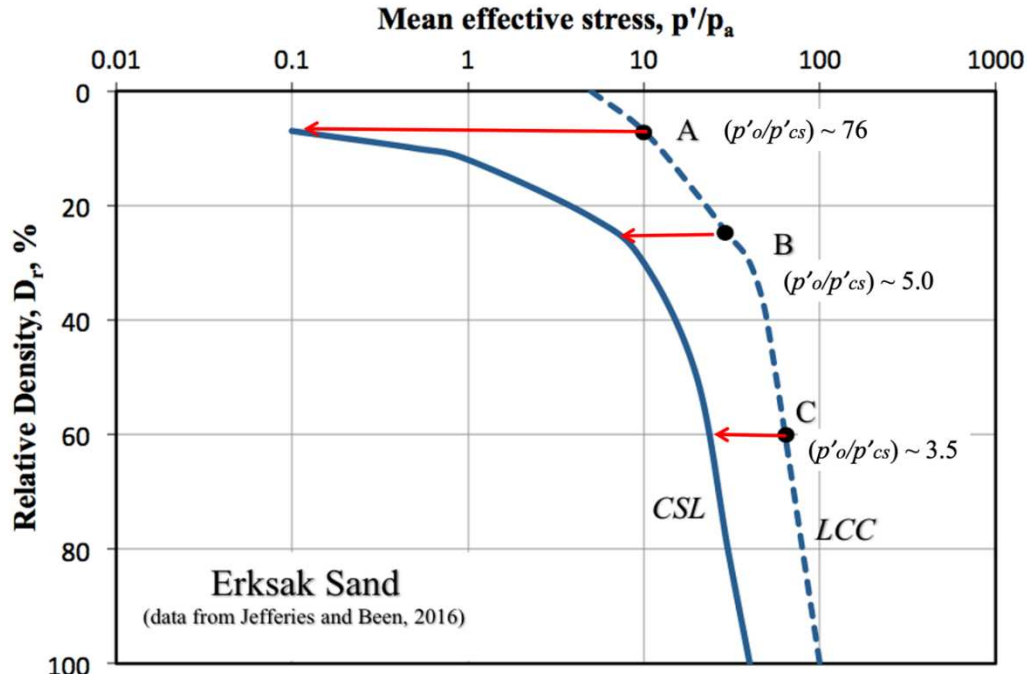


Figure 3. Critical State Line (CSL) and approximate Limiting Compression Curve (LCC) for Erksak sand (data from Jefferies and Been, 2016).

Table 1. Summary of isotropically consolidated undrained triaxial compression tests results on Erksak sand (Jefferies and Been, 2016).

Test	$\psi$	$p'_o/p_a$	$p'_o/p'_{cs}$	$Su_{(cs)}/\sigma'_{vo}$
A	0.07	10	76	0.008
B	0.20	30	5.0	0.12
C	0.25	60	3.5	0.17

The data in Table 1 show that the initial state parameter is not a good index of undrained behavior, unless the slope of the CSL is included (as shown in Equation 1). The results also show that with increasing effective confining stress, the strength loss index for Erksak sand decreases. The strength loss index ( $I_{SL}$ ) is based on the brittleness parameter ( $I_B$ ) developed by Bishop (1967), and is defined as:

$$I_{SL} = (\tau_p - \tau_r)/\tau_p \quad (5)$$

Where  $\tau_p$  is the peak strength and  $\tau_r$  is the residual strength defined under the same effective normal stress. When  $I_{SL} = 1$ , the soil has lost 100% of its strength; when  $I_{SL} = 0$ , there is no strength loss.

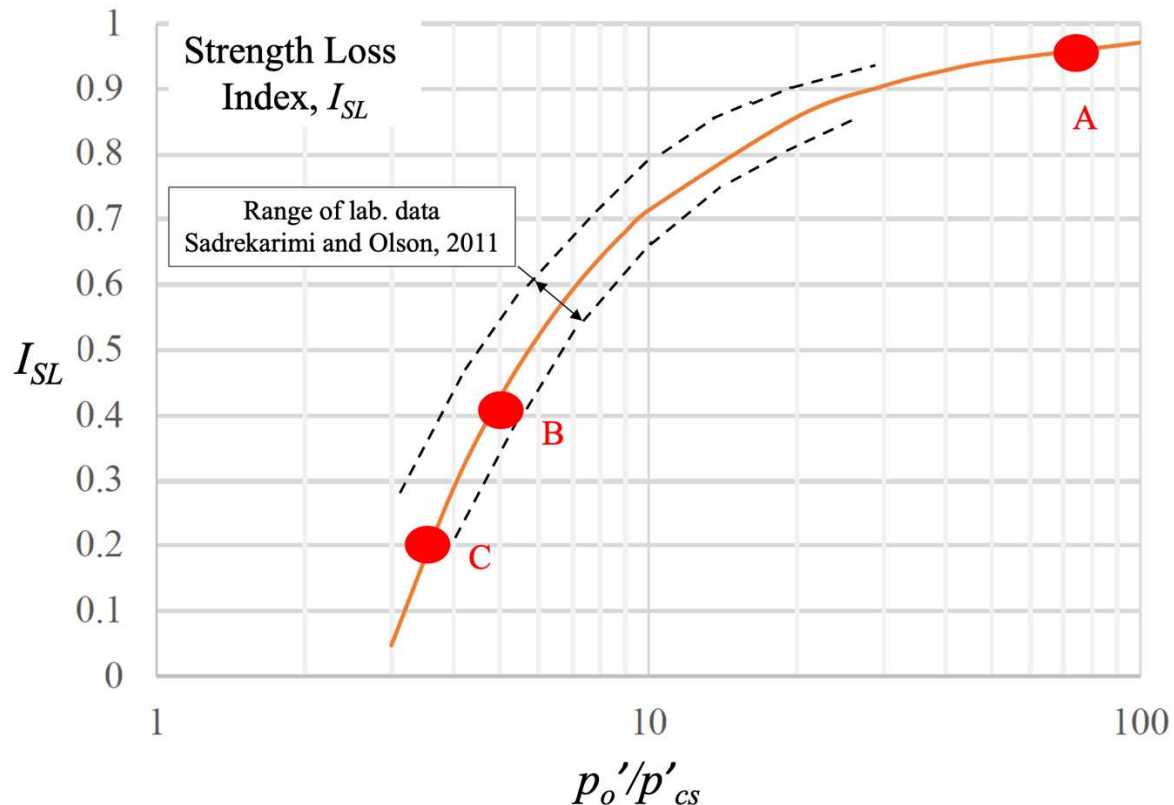


Figure 4. Strength Loss Index ( $I_{SL}$ ) versus Reference Stress Ratio ( $p'_o/p'_{cs}$ ) for a range of sands with three tests on Erksak sand added in red.

The test results on Erksak sand summarized on Figure 3 (tests A, B, and C) are plotted on Figure 4 alongside data from Sadrekarimi and Olson (2011) for several sands. Data shown on Figure 4 illustrate that for very loose contractive sand-like samples, strength loss progressively decreases, and the large strain undrained strength ratio progressively increases with increasing stress level due to the non-linear CSL and the resulting decrease in the RSR. Schnaid et al. (2013) presented data on a silty, non-plastic tailings from a gold mine in Brazil which also show the effect of the CSL curvature on limiting the strength loss index of tailings.

Table 2 compares the characteristics of the two soils (Erksak sand and the Schnaid silty tailings) and shows that Erksak sand is essentially a clean mostly quartz sand while the silty tailings are non-plastic with a fines content of around 40%, resulting in higher compressibility. The characteristics of Candelaria tailings (case history details presented later) are also summarized in Table 2.

Table 2. Summary of the main characteristics of the tested sands used in this study.

Sand	D <sub>50</sub> (mm)	Fines content (%)	Main minerals	Specific gravity (G <sub>s</sub> )	References
Erksak sand	0.33	< 1	Quartz	2.7	Jefferies and Been (2016)
Silty (gold) tailings	0.10	~40%	Quartz (32%) Albite (24%) Chlorite (23%)	3.0	Schnaid et al. (2013)
Coarse tailings (Candelaria)	0.10	40% (includes 5% clay size)	Quartz (17%) Feldspars (35%) Mica/Chlorite (35%)	3.0	Sotil et al. (2020)
Fine tailings (Candelaria)	0.03	82% (includes 12% clay size)	Quartz (19%) Feldspars (36%) Mica/Chlorite (30%)	3.0	Sotil et al. (2020)

Figure 5 presents a summary of the undrained triaxial compression test results performed on very loose (reconstituted) samples of Erksak sand and the silty tailings in terms of  $Su_{(min)}/\sigma'_{vo}$  versus  $\log(\sigma'_{vo}/p_a)$ , where  $p_a$  is the atmospheric pressure and is used to make the effective confining stress dimensionless. The relationships shown on Figure 5 used the approach described in Equation 4 to produce smooth continuous curves based on best estimates for the continuous CSLs and LCCs. The data in Figure 5 show that relatively incompressible clean silica sands (such as Erksak sand) require very high stresses (>1,000kPa) before the CSL becomes noticeably curved, and the large strain undrained strength ratio starts to increase with confining stress. However, for more compressible sands, such as the silty tailings, the CSL becomes curved at much smaller stress (less than 100kPa), as shown on Figure 1 and Figure 5; therefore, the increase in large strain undrained strength ratio occurs at lower confirming pressure relative to the clean sand. The curves are a useful method for illustrating the changes in the large strain undrained strength ratio as a function of initial effective vertical stress based on the observed non-linear CSL. Results presented on Figure 5 are from isotropically consolidated triaxial compression tests, and the relationship between the large strain undrained strength ratio in DSS (Ladd and Degroot, 2003) and effective confining stress would be slightly lower and to the right of the triaxial compression lines shown on Figure 5.

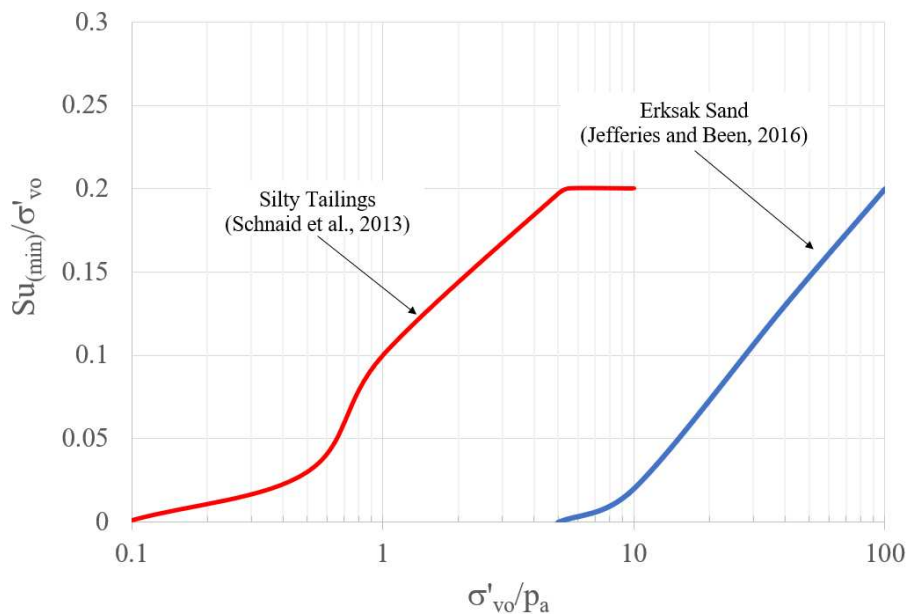


Figure 5. Variation of  $Su_{(min)}/\sigma'_{vo}$  from triaxial compression tests as a function of normalized effective confining stress ( $\sigma'_{vo}/p_a$ ) for Erksak sand (Jefferies and Been, 2016) and a silty (gold) tailings (Schnaid et al., 2013).

The overall objective of the field and laboratory test work for the Candelaria tailings case study was to evaluate the change in large strain undrained strength with increasing confining pressure and confirm that increasing the stress conditions of the shallow tailings could result in an improvement of the tailings undrained strength characteristics and hence, the overall stability of the TSF. Given that the Candelaria tailings characteristics are similar to the silty gold tailings (Schnaid et al., 2013), the expectation is that strength curves developed for the Candelaria coarse and fine tailings may bookend the silty tailings curve shown in Figure 5.

## CASE HISTORY

### Site Overview

The Candelaria Copper Mining Complex comprises two adjacent copper mining operations, Candelaria and Ojos del Salado, that produce copper concentrates from an open pit and from underground mines. The complex is indirectly owned by Lundin Mining (80%) and Sumitomo (20%). The mining complex is in Chile's Atacama Region at an elevation of approximately 650 m above sea level and 20 km south of the city of Copiapó. The Candelaria Tailings Storage Facility (TSF) ceased operations in 2019 and a surface cap will be developed for closure of the impoundment. An aerial photograph of the site is shown in Figure 6.



Figure 6. Overview of Candelaria TSF.

Ongoing mining activities will generate approximately 800 Mt of additional waste rock during future mining operations. The inactive Candelaria TSF provides an opportunity for impoundment closure capping activities to be integrated with long-term waste rock disposal during ongoing mine operations. Capping the Candelaria TSF will provide significant storage capacity for waste rock within a reasonable haulage distance from the open pit, will reduce additional site disturbances for ongoing mine operations, and will facilitate post-closure surface water management by providing a naturally appearing convex, free-draining, stable post-closure landform. The closure cap will be constructed on the surface of the Candelaria TSF by progressive placement of waste rock in layers to develop a 20 m to 60 m thick waste rock cap with flat (20H:1V) overall slopes, as shown schematically in Figure 7. The waste rock loading sequence will promote consolidation, densification, and dewatering of the underlying tailings (Sotil et al., 2020).

The Candelaria tailings have been hydraulically deposited from the perimeter of the impoundment and are somewhat layered, with coarser (sandier) materials near the discharge points and finer (siltier) tailings further from the perimeter and adjacent to the historical reclaim water pond. Field and laboratory studies investigated the tailings characteristics to facilitate prediction of tailings behavior prior to, during, and after construction of the waste rock capping layers.

Field and laboratory testing were focused on evaluating the tailings properties before and after loading. The field program involved construction of two 30 m high surcharge loads (Test Pads) on the tailings surface shortly after the Candelaria TSF

ceased operations. The approximate locations of the Test Pads in relation to the embankments and the historical tailings surface water pond are shown in Figure 6; the fully constructed Test Pads are shown in Figure 8.

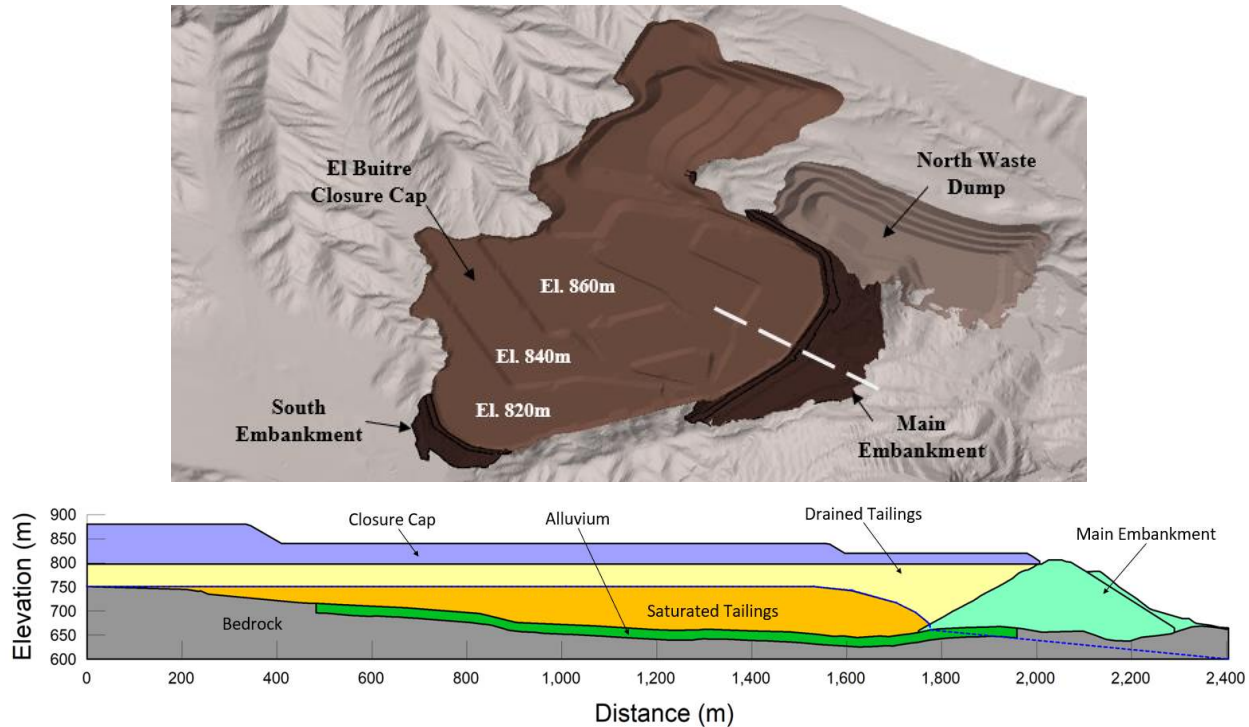


Figure 7. Plan and section of the proposed closure cap on the Candelaria TSF.



Figure 8. Isometric view of the Candelaria Test Pads.

CPT soundings and sampling drillholes were advanced through the tailings before and after pad construction to evaluate the change in tailings characteristics due to the surcharge load. Laboratory testing was subsequently completed on reconstituted tailings samples to refine the undrained shear strength estimates developed from the CPT data.

### Site Investigation Program

Site investigations were completed on the surface of the deactivated tailings impoundment (to depths of up to 150 m) before and after construction of the Test Pads, with the investigations focused on evaluating tailings improvements due to loading, including changes in the undrained shear strength properties of the tailings.

The Test Pads had a central diameter at the crest of about 70 m with average side slopes of 2H:1V, over a 6 m thick base of about 280 m in diameter. These Test Pads simulated the staged loading that will occur during ongoing development of the closure cap, with Test Pad 1 constructed on a relatively competent area of the coarser tailings beach, and Test Pad 2 constructed on finer grained saturated tailings adjacent to the historical reclaim water pond, as illustrated in Figures 6 and 8. The Test Pads experienced total settlement of about four meters at Test Pad 1 and six meters at Test Pad 2. Settlements and excess pore pressure dissipation from pad loading were complete within four months after pad construction.

The site investigations at the Test Pads are schematically illustrated in Figures 9 and 10, and incorporated sonic drilling, sample collection, installation of vibrating wire piezometers, and seismic CPT (SCPT) investigations. The post-loading SCPTs and drillholes were carried out after construction-induced excess pore pressures were fully dissipated.

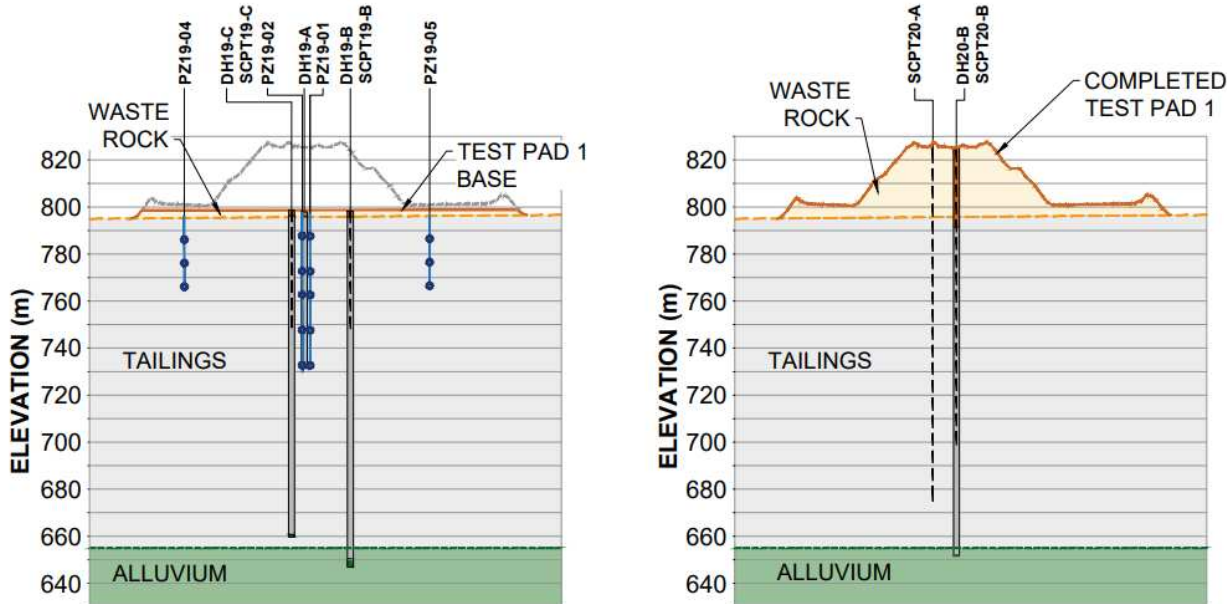


Figure 9. Tailings site investigations at Test Pad 1 before (left) and after (right) pad construction.

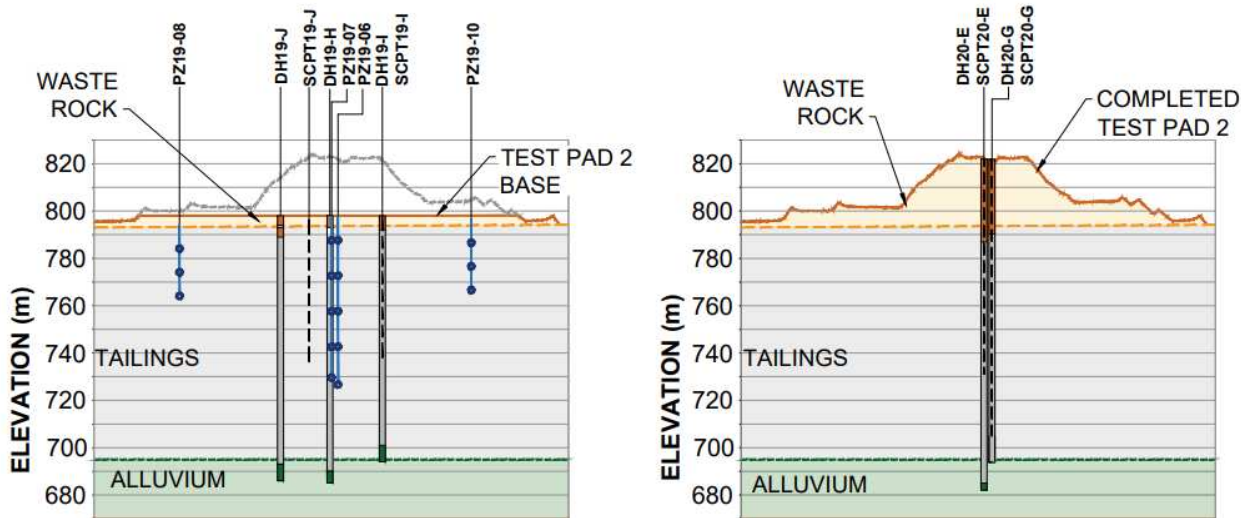


Figure 10. Tailings site investigations at Test Pad 2 before (left) and after (right) pad construction.

The equilibrium pore pressure conditions in the tailings, as shown in Figure 11, were determined from vibrating wire piezometer (VWP) measurements and CPT pore pressure dissipation (PPD) tests. The VWPs were installed at various depths within the tailings to monitor excess pore pressures during Test Pad construction. The PPD tests were carried out at

approximately five-meter intervals before and after Test Pad construction and were run to equilibrium. Results of the PPD tests indicate that the Candelaria tailings are relatively permeable, with  $t_{50}$  values of less than twenty seconds measured at both Test Pad locations. However, the high positive pore pressures measured during CPT penetration indicate a predominately contractive undrained response during the CPT in the finer tailings. The equilibrium pore pressure profiles were determined during Phase 1 (before pad construction) and Phase 2 (after pad construction) site investigation programs.

In general, the tailings were found to be draining downwards toward the pervious basal alluvium deposit (Figures 7 and 11), with pore pressure conditions found to be significantly less than hydrostatic. The tailings below the phreatic surface are saturated with downward flow. Active downward flow was also measured by the VWP instrumentation during the 2-year construction and monitoring period, with a drop in the phreatic surface measured at approximately 0.5 meters/month at both Test Pad locations. The downward flow is also evident in the piezometric profiles that were developed before and after construction of the Test Pads. The equilibrium pore pressure profiles were used to determine effective stresses within the tailings at the time of each investigation.

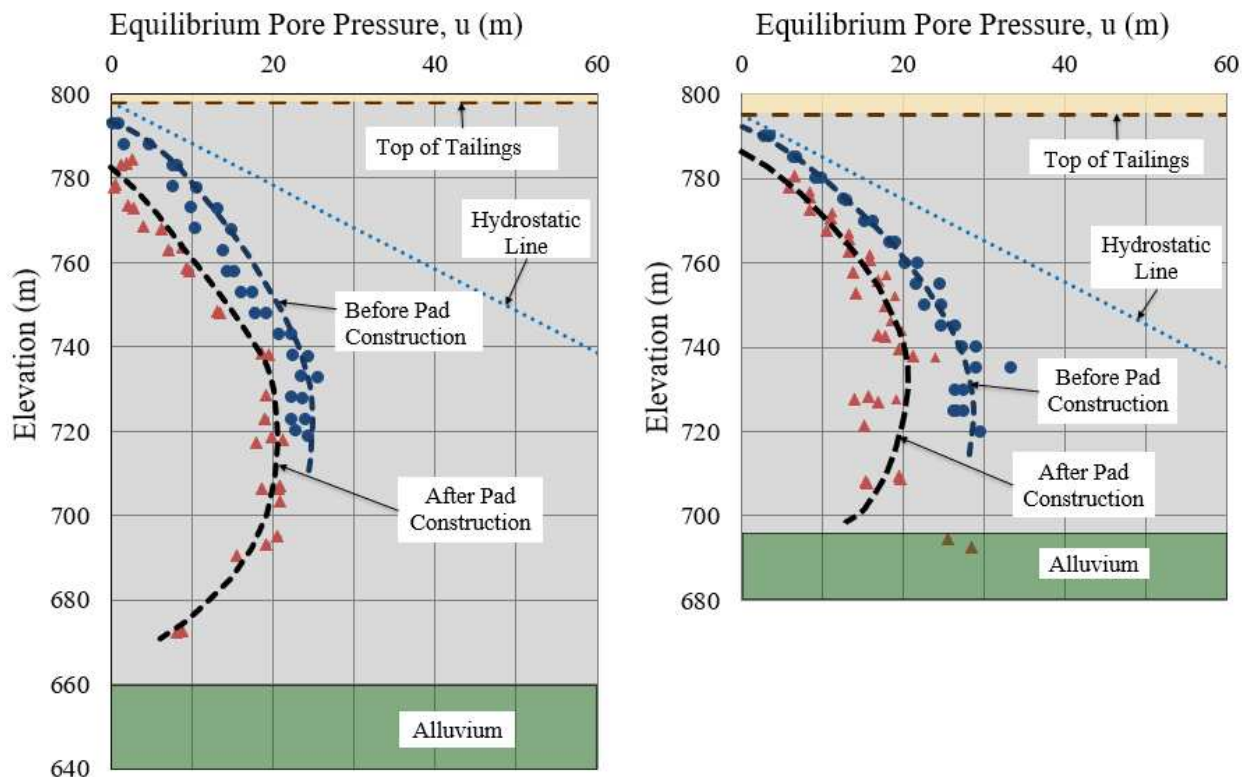


Figure 11. Pore pressure profiles at Test Pad 1 (left) and Test Pad 2 (right) from PPD tests.

SCPT profiles were obtained in the tailings at both Test Pad locations before and after pad construction. The SCPTs at each Test Pad location were advanced within approximately 25 m of each other. Example SCPT raw data profiles (before and after pad construction) are shown in Figures 12 (Test Pad 1) and 13 (Test Pad 2) and illustrate profiles of the tip resistance ( $q_t$ ), sleeve friction ( $f_s$ ), friction ratio ( $R_f$ ), and dynamic pore pressure ( $u$ ) by elevation. Figures 14 (Test Pad 1) and Figure 15 (Test Pad 2) provide profiles of tip resistance, normalized cone resistance ( $Q_{tn}$ ), shear wave velocity ( $V_s$ ), and normalized shear wave velocity ( $V_{s1}$ ) by elevation, to examine the improved tailings response after pad construction. The normalized cone-resistance values were filtered as mean values over one-meter intervals to reduce the scatter in the data.

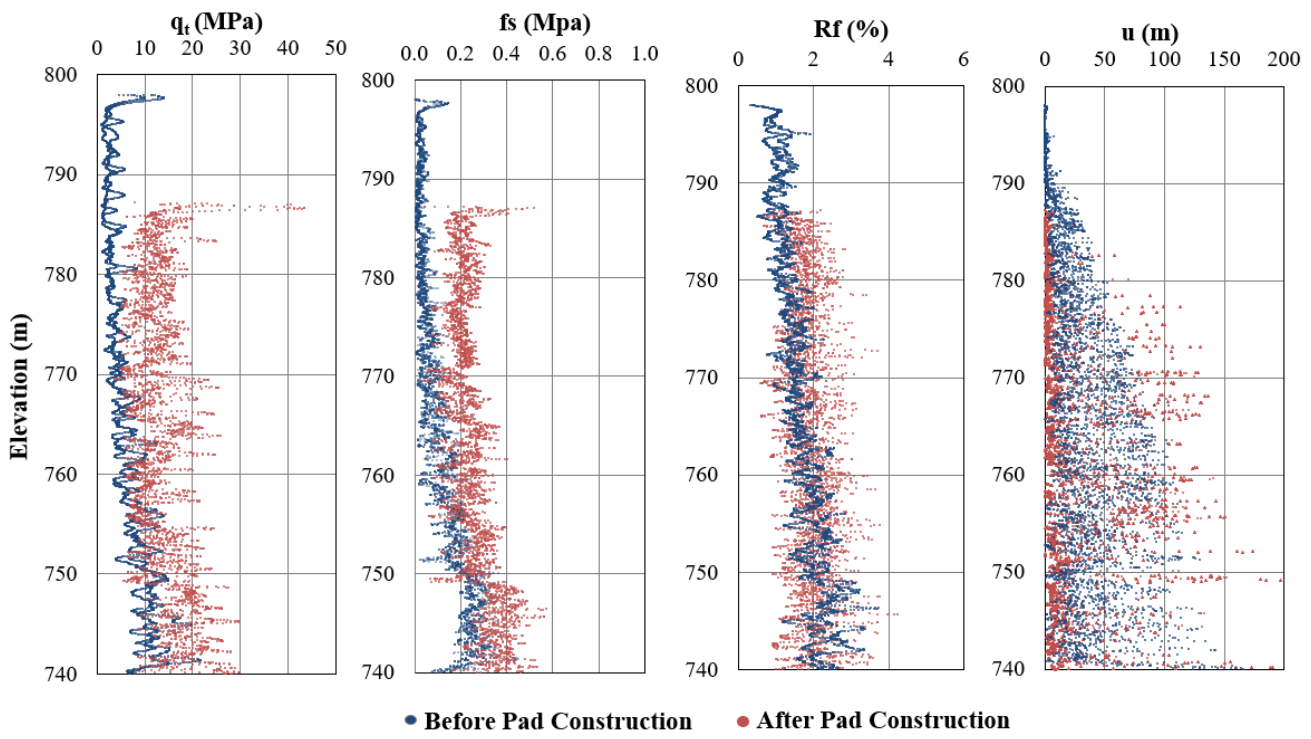


Figure 12. Raw SCPT data before and after construction of Test Pad 1.

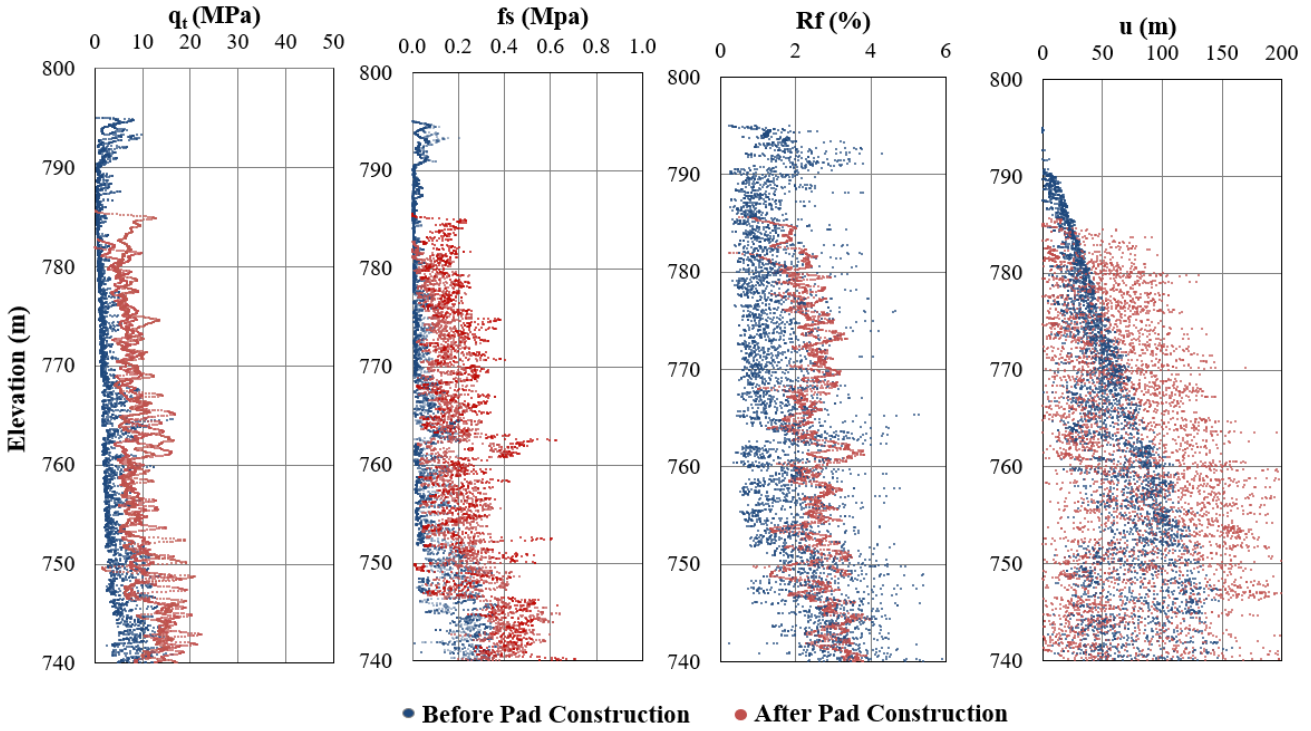


Figure 13. Raw SCPT data before and after construction of Test Pad 2.

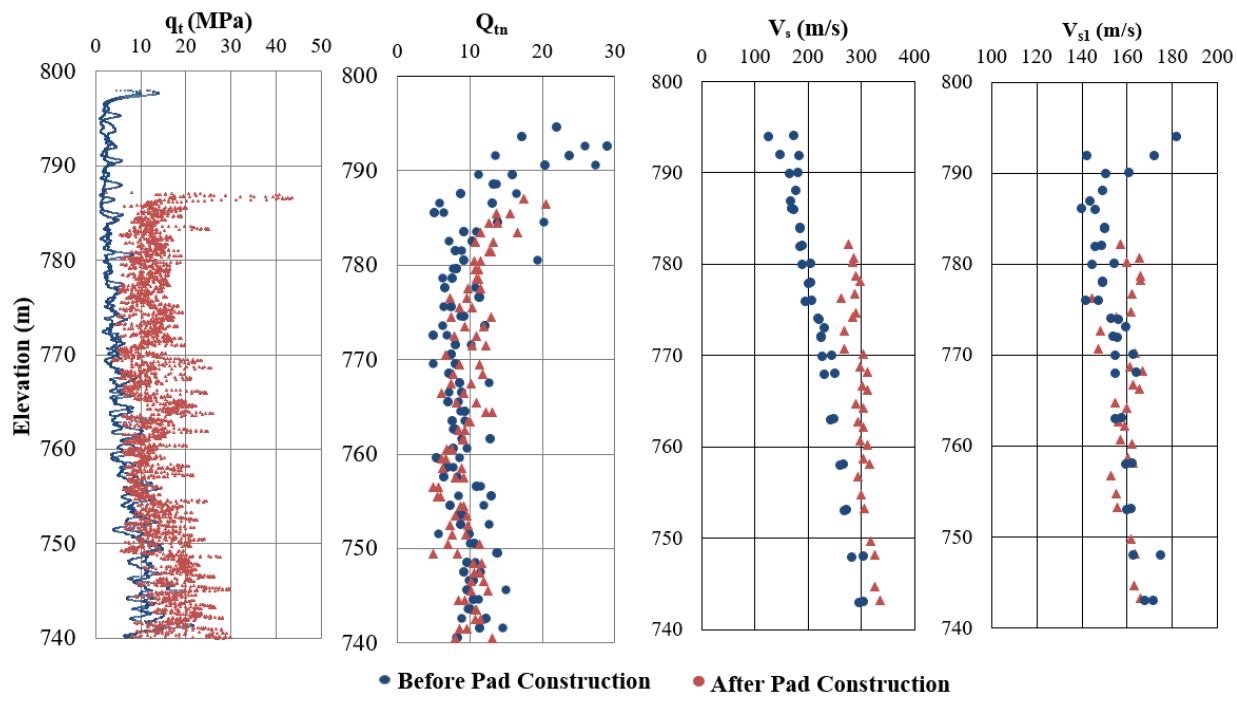


Figure 14. SCPT data before and after construction of Test Pad 1.

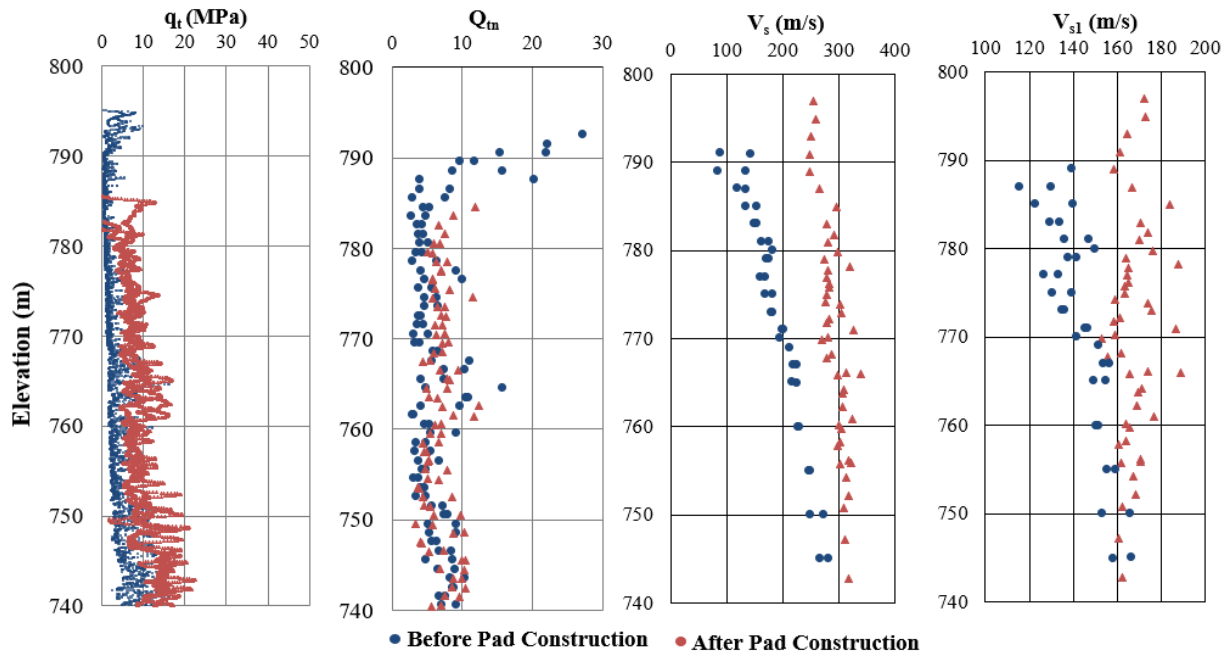


Figure 15. SCPT data before and after construction of Test Pad 2.

The SCPT data at both Test Pad locations show significant increases in the tailings resistance and stiffness after Test Pad construction. Increases in confining pressure would be expected to result in an increase in the material stiffness, as reflected in the raw tip resistance, sleeve friction, and shear wave velocity measurements. However, the SCPT data also show an increase in the stress-normalized tip resistance and shear wave velocity measurements above elevation (EL.) 760 m, which indicates an improvement in the in-situ density and state of the shallower tailings.  $Q_{tn}$  values in the upper 30 m of saturated tailings generally increased after Test Pad construction from 7 to 12 and from 4 to 7 at Test Pad 1 and 2, respectively. Robertson (2021) presented a revised methodology for estimating the residual (liquefied) undrained shear strength ratio for

contractive materials using the CPT measured  $Q_{tn}$  parameter corrected for soil compressibility. Therefore, the increase in  $Q_{tn}$  values indicates that surcharge loading resulted in an increase in the residual undrained shear strength ratio for the tailings materials (Figure 18), and these improvements were more pronounced in the shallower tailings which experienced the greatest relative confining stress increase due to pad construction. The relative changes in  $Q_{tn}$  were also greater for the finer tailings encountered at Test Pad 2, suggesting a larger improvement in the tailings residual strength ratio relative to the coarser tailings at Test Pad 1.

The combined shear wave velocity ( $V_s$ ) and CPT data indicate that the tailings have no microstructure based on the methodology suggested by Robertson (2016) where the average  $K^*_G$  (normalized rigidity index) values are around 200. Given the lack of any microstructure in the tailings, the updated method suggested by Robertson (2021) is considered appropriate for estimating the large strain minimum undrained strength ratio of the contractive tailings.

Robertson (2021) presented contour lines of the minimum undrained strength ratio on the normalized Soil Behavior Type ( $SBT_n$ ) as incorporated in Figures 16 and 17. The  $SBT_n$  chart includes the  $CD = 70$  line which provides an approximate boundary between contractive (below the  $CD = 70$  line) and dilative materials (above the  $CD = 70$  line). In general, materials that plot below but near the  $CD = 70$  line have higher residual undrained shear strengths than materials that plot further below this boundary, as illustrated by the contours of minimum undrained strength ratio. The CPT data collected at Test Pads 1 and 2 were plotted as point density contours on the  $SBT_n$  charts, as shown in Figures 16 and 17. CPT data were filtered to include the saturated tailings above elevation (EL.) 763 m (which corresponds to approximately the upper 30 m of saturated tailings at each Test Pad location) as these are the loosest materials that experience the largest incremental change after Test Pad construction. The contouring in Figures 16 and 17 uses 2D Gaussian Kernel Density Estimation (KDE) over a log-log-transformed scale mapped back onto the plotting area to provide an estimate of the probability density for each  $SBT_n$  dataset. Contouring was defined to show zones with higher point densities in hot (red) colors, and zones with lower point densities in cold (blue) colors. Common color bars were defined for each of the Test Pads to illustrate the change in the data after loading. The color bars represent the approximate unit probability density of the data within the plotting area.

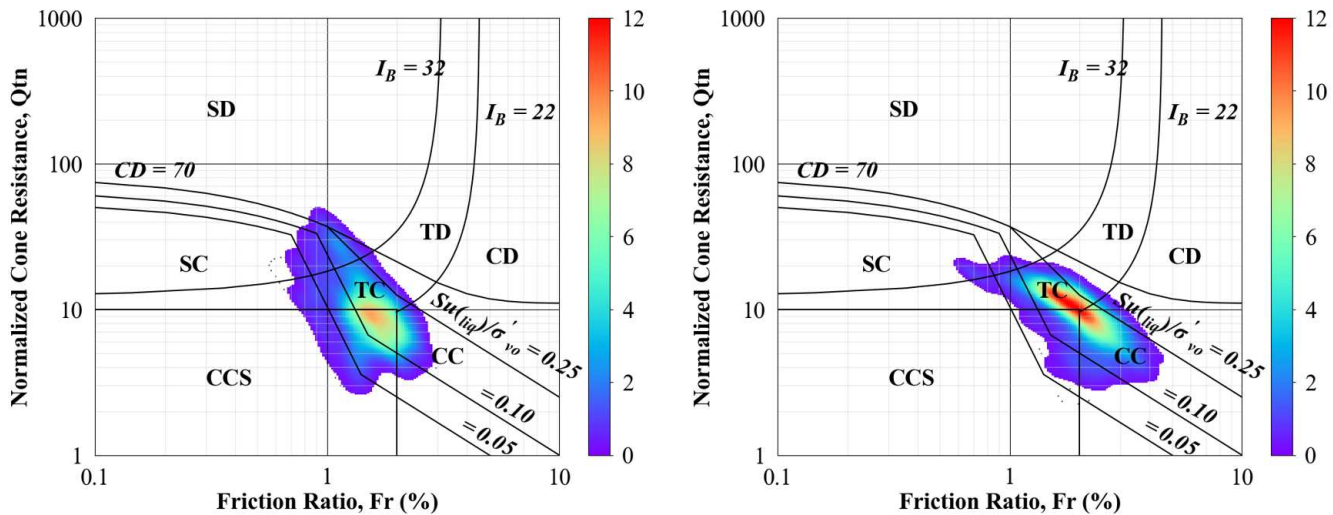


Figure 16.  $SBT_n$  plots for Test Pad 1 with contours of  $Su_{(min)}/\sigma'_{vo}$  before (left) and after (right) Test Pad loading (for saturated tailings above EL. 763 m).

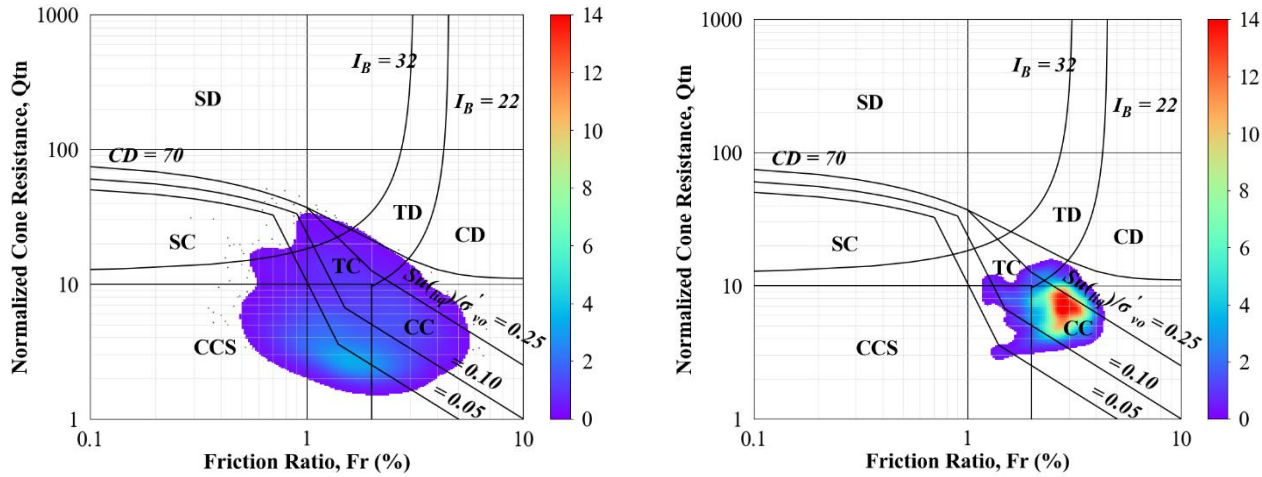


Figure 17. SBT<sub>n</sub> plots for Test Pad 2 with contours of  $Su_{(min)}/\sigma'_{vo}$  before (left) and after (right) Test Pad loading (for saturated tailings above EL. 763 m).

The SBT<sub>n</sub> point density contours illustrate the improvement in the residual undrained shear strength ratio of the tailings after loading, further supporting the observations made from the CPT profiles presented in Figures 14 and 15. Figure 16 shows the loosest CPT data points at Test Pad 1 shifting upwards towards the CD = 70 contractive-dilative boundary after surcharge loading. This change is evident in both the shape of the contour plot (more data above the 0.1 residual strength contour line) and the size and shape of the higher frequency (red) contour (close to and approximately parallel to the 0.25 residual strength contour line). The upwards shift indicates that the loose tailings layers below Test Pad 1 were improved and densified by the surcharge load. Figure 17 shows a more pronounced change in the SBT<sub>n</sub> isopach at Test Pad 2, which is reasonable given the initial looser state of the finer tailings near the historical reclaim pond area. The residual undrained shear strength ratio estimated from these SBT<sub>n</sub> plots is shown to have increased, and the dataset shifted from relatively uniform distribution of data (before loading) to a more condensed data set with a higher interpreted residual undrained shear strength after loading.

The change in residual undrained strength ratio of the saturated tailings above EL. 763 m as illustrated on the SBT<sub>n</sub> charts, were further investigated using the recently updated residual shear strength ratio equations developed by Robertson (2021). Values of the residual undrained strength ratio were estimated from the CPT data and plotted as a function of the in-situ vertical effective stress at the time the CPT sounding was performed. Figure 18 shows the change in the residual (liquefied) undrained strength ratio as a function of in-situ vertical effective stress at Test Pads 1 and 2. The CPT data were filtered by aggregating data points over 2.5 m depth intervals and determining a 30<sup>th</sup> percentile residual undrained strength ratio over that depth interval. Data presented in Figure 18 incorporate the saturated tailings above EL. 763 m before and after loading, and show a clear increase in the residual undrained shear strength ratio as a result of Test Pad construction at both locations. The change in vertical effective stress due to pad construction was estimated based on the unit weight and thickness of the Test Pad. An influence factor of 1 was assumed below the Test Pads, which is considered reasonable since the diameter of the Test Pad crests were 70 m at both locations. Any errors in the influence factor (e.g., if the true influence factor is less than 1) would mean that the interpreted residual (liquefied) undrained shear strength ratios, which are estimated from stress normalized parameters, are slightly conservative. The dotted lines in Figure 18 illustrate the general bounds of the data, and the dashed line is used to illustrate the average of the dataset. These data bounds (shaded region) and averages (dashed line) are used in Figures 19 and 22 to allow the trends in the SCPT data to be compared to laboratory testing data.

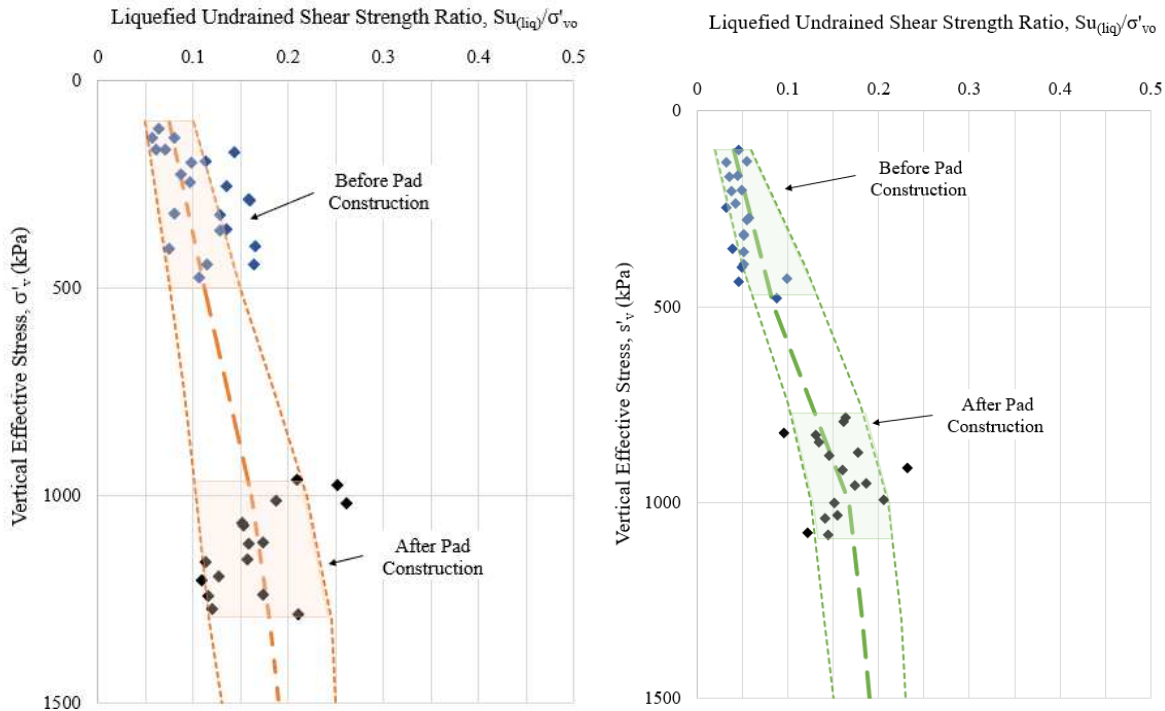


Figure 18. Variation of residual (liquefied) undrained strength ratio from CPT interpretation as a function of vertical effective stress at Test Pad 1 (left) and Test Pad 2 (right).

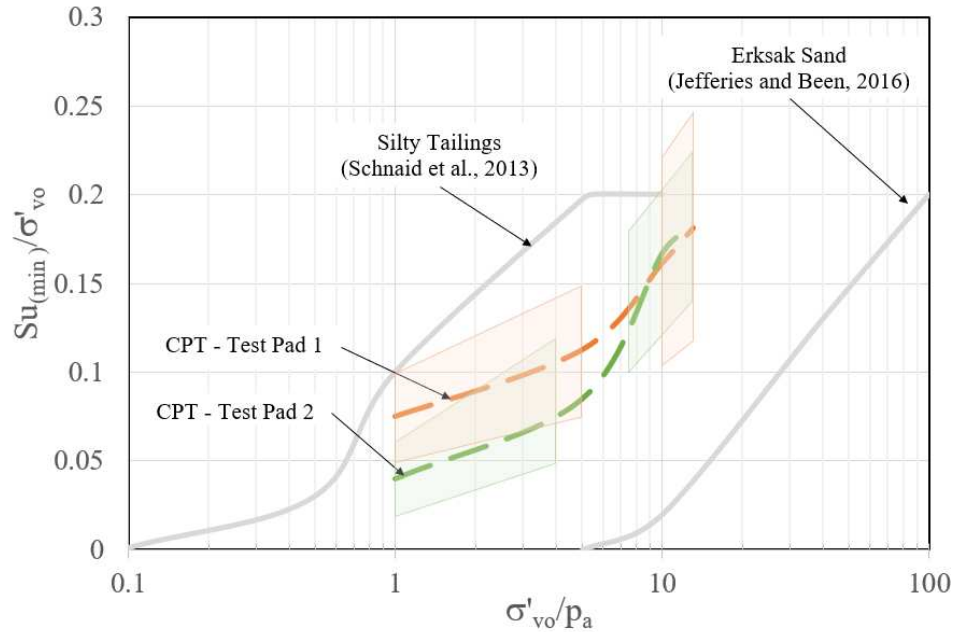


Figure 19. CPT interpretation of  $Su_{(min)}/\sigma'_{vo}$  compared to the lab derived curves for Erksak sand and the silty tailings (Schnaib et al., 2013) versus  $\log(\sigma'_{vo}/p_a)$ .

The change in the large strain undrained strength ratio, as indicated by the increase in  $Su_{(min)}/\sigma'_{vo}$  from CPT data, is also represented as a function of normalized effective confining stress ( $\sigma'_{vo}/p_a$ ) as shown in Figure 19, where the large strain undrained strength ratio relationships from the Candelaria tailings CPT data are compared to the laboratory test data presented earlier for Erksak sand and the Schnaib silty gold tailings.

## Laboratory Testing

The Candelaria tailings are essentially non-plastic with a mineralogy composed of about 15 to 20% quartz, 35% feldspar minerals, 30 to 40% mica/chlorite, with 5 to 8 % clay (smectite), as summarized in Table 2.

The particle size distributions for multiple tailings samples collected from various depths at Test Pads 1 and 2 are illustrated in Figure 20. Laboratory tailings samples were prepared by selectively separating and blending tailings to generate coarse sandy tailings and fine silty tailings sample blends, as highlighted in Figure 20. The individual reconstituted samples are not strictly representative of the in-situ layered tailings materials below each of the test pads but provide general bounding conditions for the CSL laboratory testing. In general, the coarse sandy tailings were intended to be more representative of the predominate materials under Test Pad 1, and the fine silty tailings more representative of the predominate materials under Test Pad 2. The individual particle size distribution curves show that the Candelaria tailings are relatively well graded. Laboratory strength testing was completed on each of the two sample blends to define the CSLs and evaluate the impact of confining pressure on the minimum undrained shear strength of the tailings.

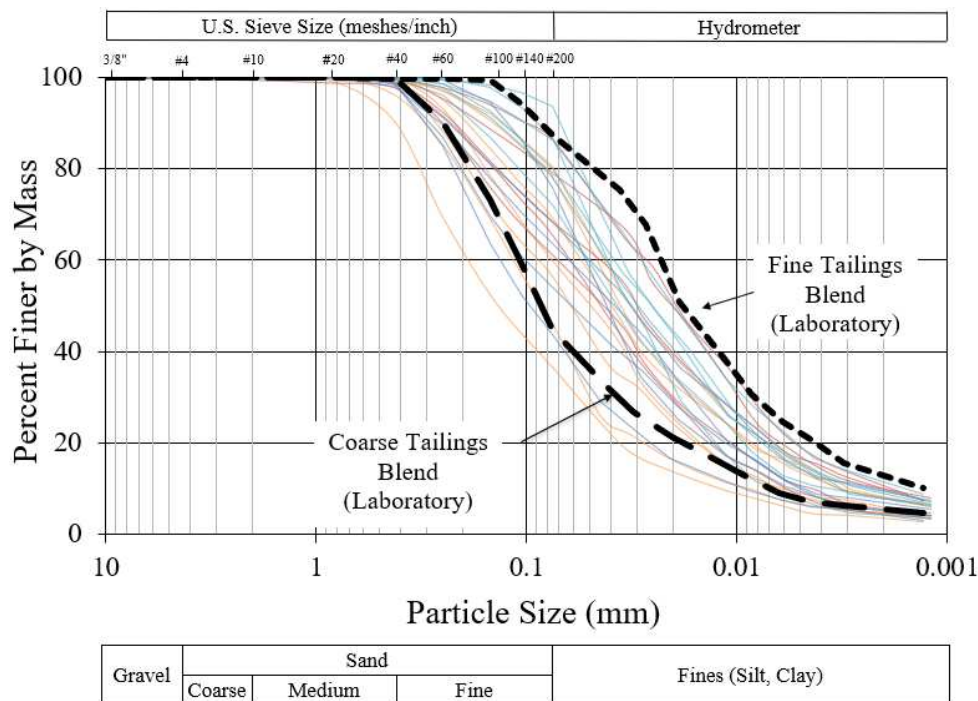


Figure 20. Candelaria tailings gradation envelope with representative reconstituted laboratory samples.

The coarse and fine tailings samples were prepared to the loosest possible state (using moist tamping) and subjected to isotropically consolidated undrained triaxial compression testing to define the CSL at low and high stresses, as illustrated in Figure 21.

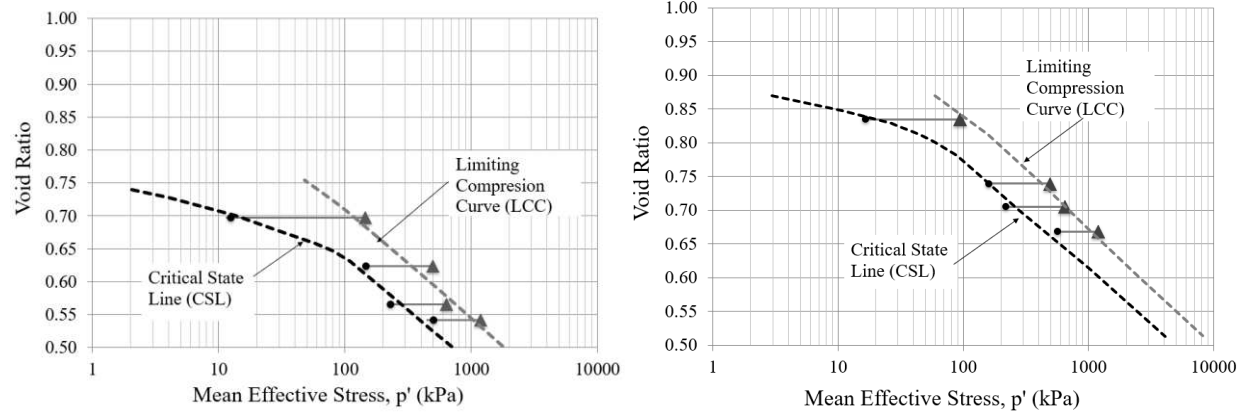


Figure 21. Curved CSLs for Coarse (left) and Fine (right) laboratory tailings samples.

Triaxial compression test results were used to develop curved CSLs, LCCs, and the slope of the CSL ( $M_{tc}$ ) for both the coarse and fine tailings by measuring the stress path during shearing. The triaxial samples were sheared to axial strains of at least 20% and all samples were interpreted to achieve CS based on the stress-strain and pore pressure response. Accurate determination of the sample void ratios was achieved by freezing the samples after shearing, where possible, which allowed for accurate determination of the CSL and LCC. Two samples of coarse tailings materials and two samples of the fine tailings materials were consolidated using a triaxial cell capable of conducting Bender Element tests. The void ratio data collected during the consolidation stages and the frozen specimens were used to define the LCC of the very loosely prepared tailings.

The offset between the LCC and the CSL (i.e., the RSR) were used to calculate the minimum undrained shear strength ratio at CS ( $S_u_{(min)}/\sigma'_{vo}$ ) over a wide stress range for the Candelaria tailings using Equation 4, and are compared to the lines for Erksak sand and the Schnaid silty gold tailings, as shown in Figure 22. The Candelaria minimum strength curves are shown in orange (coarse tailings) and green (fine tailings) with circular markers shown for the independent triaxial data points. Curves for the Candelaria tailings are very similar to the silty gold tailings (Schnaid et al., 2013) with the fine tailings (80% fines content) plotting slightly to the left and the coarse tailings (40% fines content) plotting slightly to the right of the reference silty gold tailings (40% fines content). Based on the similar mineralogy and fines content between the Candelaria tailings and the Schnaid silty gold tailings (see Table 2), it is reasonable to expect good agreement between the curves.

A small number of constant volume direct simple shear (DSS) tests were also carried out on the Candelaria tailings at two effective vertical consolidation stresses (500 and 1,000 kPa). The values of the minimum undrained shear strength ratio from the DSS tests were about 20% lower than those from the triaxial compression tests, which is consistent with other published data for non-plastic sands and silts at the differing modes of shear. The DSS test results are plotted using square markers in Figure 22. The CPT interpreted mean minimum undrained strength relationships from Test Pad 1 and Test Pad 2 as presented in Figure 19 are also included in Figure 22 to compare the field and laboratory derived data.

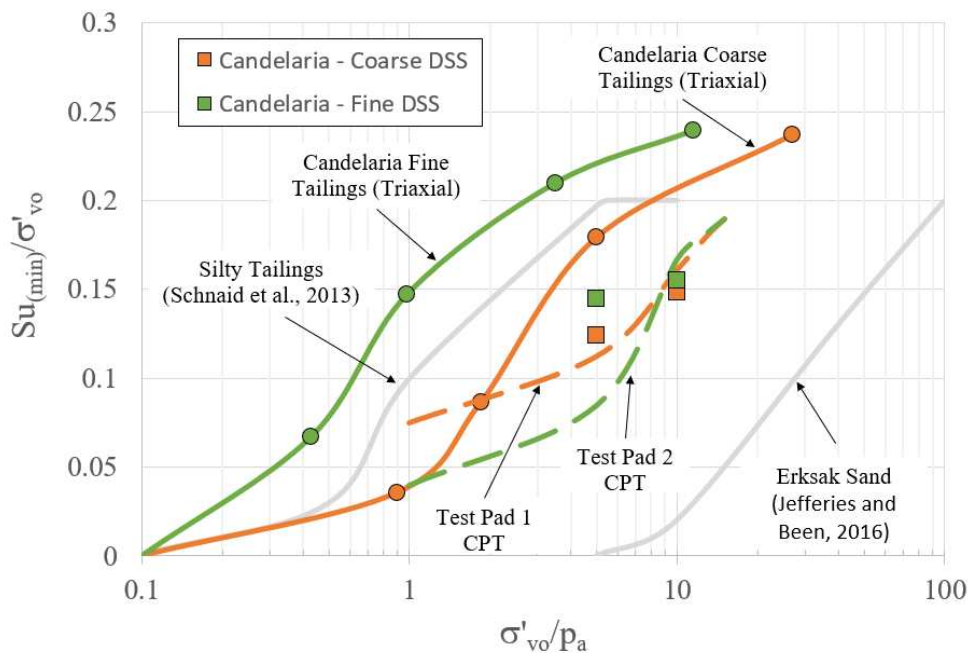


Figure 22. Variation of  $Su_{(min)}/\sigma'_{vo}$  for Candelaria tailings as a function of normalized effective confining stress ( $\sigma'_{vo}/p_a$ ), (with reference to Erksak sand and Schnaid silty tailings).

## DISCUSSION

Figure 22 compares the laboratory and CPT results from the Candelaria Test Pads relative to previously published trends. The CPT interpreted values agree very well with the limited DSS test results. The CPT residual undrained shear strength equations (Robertson, 2021) were developed mainly from back-analyses of case histories where failure modes tend to be dominated by the DSS direction of loading which may explain the general good agreement observed. It is encouraging that the CPT-based correlations worked well over the wide stress range at this site. The Candelaria tailings also have similar grain characteristics to the silty gold tailings tested by Schnaid et al. (2013) and the results show a very similar trend.

The location of the relationship between  $Su_{(min)}/\sigma'_{vo}$  and  $(\sigma'_{vo}/p_a)$  appears to be controlled by the compressibility of the material, with uniform rounded to sub-rounded silica sands (such Toyoura and Erksak sands) that have a low compressibility plotting to the right at very high stresses ( $> 1,000$  kPa) and silty sands that have a higher compressibility plotting more to the left at much lower stresses ( $< 500$  kPa). Jefferies and Been (2016) suggested that the slope of the CSL ( $\lambda_{10}$ ) over a stress range of about 100 to 300 kPa can be used as a measure of compressibility. Plewes et al. (1992) and Reid (2014) showed that there is also a link between either normalized friction ratio ( $F_r$ ) or SBT index ( $I_c$ ) and  $\lambda_{10}$ , and that these CPT parameters can be used as a proxy for compressibility. Robertson (2017) suggested that the variation in the large strain  $Su_{(min)}/\sigma'_{vo}$  from a more brittle response with large strength loss ( $I_{SL} > 0.5$ ) to a more ductile response with smaller strength loss ( $I_{SL} < 0.5$ ) can be estimated using  $F_r$ , as shown in Figure 23. Figure 23 includes the case history data from Robertson (2010), as well as the trend from Candelaria testwork that also matches the general observations. The Candelaria CPT data is generally observed to have a normalized friction ratio between 1 and 3. Therefore, based on the case history data and relationship suggested by Robertson (2017), it would be expected that the strength loss potential of the tailings would reduce with increasing stress level. The data presented in Figure 23 further supports the improvement in the tailings residual strength observed in the SCPT and laboratory data.

The presented data are from soils with no microstructure. Research on very sensitive (quick) clays and lightly bonded sands has shown that these soils can have significant microstructure that can influence strength loss and brittleness. It is likely that lightly bonded soils may continue to have significant strength loss (i.e., high strength loss index) for effective confining stresses below the yield stress and, that when the confining stresses exceed yield, there may be a link between confining stress and minimum undrained strength ratio, similar to the results shown for unstructured soils.

High strength loss potential occurs in very loose soils at low confining stress. This indicates that the most critical region of tailings structures is likely to be close to the toe of embankments where effective confining stresses can be low and piezometric surfaces can be high. This also supports the observation that observed flow liquefaction failures tend to be retrogressive in nature with multiple shallow failure surfaces (e.g., Robertson et al., 2019).

The field and laboratory data collected at the Candelaria Mine builds on existing data and further demonstrates that the strength loss potential of loose soils, particularly in sandy silt to silty sand materials, can be significantly improved by increasing the stress state of the loose materials. Site specific application of economic ground improvement technologies, such as buttressing and surcharge loading, can be considered as practicable mitigation measures to improve the strength-loss potential of loose materials susceptible to flow liquefaction.

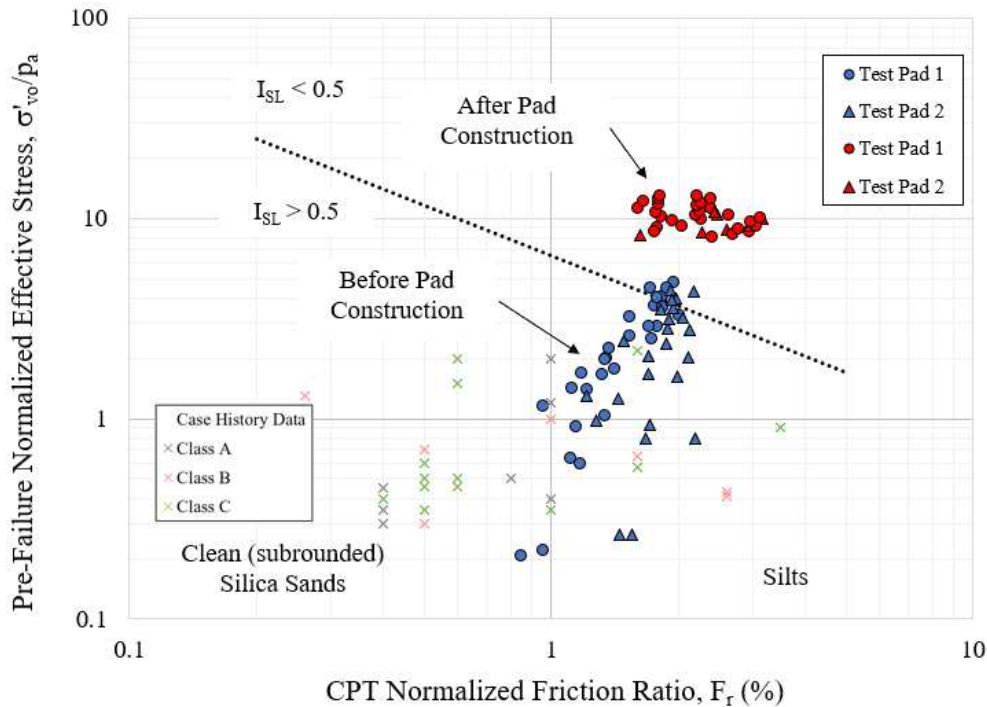


Figure 23. Variation in large strain undrained behavior as a function of CPT normalized friction ratio ( $F_r$ ) (modified from Robertson, 2017, case history data from Robertson, 2010).

## CONCLUSION

Field and laboratory measurements of the Candelaria tailings have provided unique data to evaluate the influence of increased confining stress on the large strain undrained shear strength of loose tailings. Published laboratory data to determine the CSL over a wide stress range was used to create a framework on how the undrained behavior should change with increasing confining stress for very loose sand-like soils. The laboratory data show that the CSL is non-linear over a wide stress range and that the non-linearity plays an important role in observed behavior for very loose sands. This was supported by the laboratory tests results from the case history. The laboratory data show that clean silica sands tend to have lower compressibility and require large changes in effective confining stress before any curvature in the CSL and resulting change in undrained behavior is observed. However, sands with higher fines content tend to have higher compressibility where the CSL becomes curved and steeper at relatively low stress and require much smaller changes in effective confining stress to observe significant changes in undrained behavior. The laboratory testing on the Candelaria tailings also showed that the undrained strength ratio in DSS loading is lower than that observed in triaxial compression loading, which is consistent with past research.

The Candelaria case history provided valuable SCPT data from the underlying tailings materials, both before and after loading from the test pads. The SCPT data were interpreted using the recently updated approach by Robertson (2021) and showed trends consistent with the laboratory data, especially with respect to the DSS results. Good agreement between the SCPT and



---

DSS data is encouraging, as the Robertson (2021) interpretation method is based primarily on past case history failures where DSS is likely the dominant loading condition. Field and laboratory data collected at Candelaria demonstrate that surcharge loading is an effective means to enhance the residual undrained shear strength of the tailings.

## ACKNOWLEDGEMENTS

We would like to acknowledge Victor Soto and the Candelaria Mine team for conducting the challenging field work and for making the Test Pad program possible. The contributions of Graham Greenaway and Julie Castellanos of Knight Piésold to the field and laboratory programs are also greatly appreciated.

## REFERENCES

Been, K., and Jefferies, M.G. (1985). "A state parameter for sands." *Géotechnique*, 35(2), 99–112.

Berti, M., R. Genevois, and Tecca, P.R. (1997). "The 1985 flow slide and debris flow at Stava (Italy)." *1st International Conference on "Debris Flow Hazard Mitigation: Mechanics, Prediction and Assessment"*, San Francisco (Cal.), ed. Chen Cheng-Jung, ASCE, New York, 309–321.

Bishop, A.W. (1967). "Progressive failure – with special reference to the mechanism causing it." *Proc. Geotechnical Conf.*, Oslo, Vol.2, 142–150.

Bolton, M.D. (1986). "The strength and dilatancy of sands." *Geotechnique*, 36(1), 65–78.

Boulanger, R.W. (2003). "High overburden stress effects in liquefaction analyses." *J. Geotechnical and Geoenvironmental Eng.*, ASCE 129(12), 1071–1082.

Jefferies, M.G., and Been, K. (2016). *Soil liquefaction – a critical state approach*. Taylor & Francis, London, ISBN 0-419-16170-8, 478 pages.

Konrad, J.-M., and Watts, B.D. (1995). "Undrained shear strength for liquefaction flow failure analysis." *Canadian Geotechnical Journal*, 32, 783–794.

Ladd, C.C., and DeGroot, D.J., (2003). "Recommended Practice for Soft Ground Site Characterization: Arthur Casagrande Lecture." *12th Pan-American Conference on Soil Mechanics and Geotechnical Engineering*, Massachusetts Institute of Technology, Cambridge, MA.

Ladd, C.C., Foott, R., Ishihara, K., Schlosser, F., and Poulos, H.G. (1977). "Stress-deformation and strength characteristics. State-of-the-art-report." *Proceedings 9th International Conference on Soil Mechanics and Foundation Engineering*, Tokyo, 2, 421–94.

Leroueil, S., and Hight, D.W. (2003). "Behaviour and properties of natural soils and soft rocks." *Characterisation and engineering properties of natural soils*, Edited by Tan et al. Swets and Zeitlinger, 29–253.

Lunne, T., Robertson, P.K., and Powell, J.J.M. (1997). *Cone penetration testing in geotechnical practice*, Blackie Academic, EF Spon/Routledge Publ., New York, 1997, 312 pages.

Mesri, G. (1975). "New design procedure for stability of soft clays discussion.", *J. of the Geotech. Eng. Div.*, ASCE, 101(4), 409–412.

Morgenstern, N.R., Vick, S., Viotti, C.B., and Watts, B.D. (2016). "Report on the immediate causes of the failure of the Fundao Dam." *Fundao Tailings Dam Review Panel*, <<http://fundaoinvestigation.com>>

Pestana, J.M., and Whittle, A.J. (1995). "Compression model for cohesionless soils." *Géotechnique*, 45(4), 611–633.

Plewes, H.D., Davies, M.P., and Jefferies, M.G. (1992). "CPT based screening procedure for evaluating liquefaction susceptibility." *Proceedings of the 45th Canadian Geotechnical Conference*, Toronto, Ont., 4, 1–9.

Reid, D. (2014). "Estimating slope of critical state line from cone penetration tests – an update." *Canadian Geotechnical Journal*, 52, 46–57.

Robertson, P.K. (2009). "Interpretation of cone penetration tests – a unified approach." *Canadian Geotechnical Journal*, 46, 1–19.

Robertson, P.K. (2010). "Evaluation of flow liquefaction and liquefied strength using the cone penetration test." *Journal of Geotechnical and Geoenvironmental Engineering*, ASCE, 136(6), 842–853.

Robertson, P.K. (2016). "Cone Penetration Test (CPT)-based soil behavior type (SBT) classification system – an update." *Canadian Geotechnical Journal*, 53(12).

Robertson, P.K. (2017). "Evaluation of flow liquefaction: influence of high stresses." *3rd International Conference on Performance Based Design in Earthquake Geotechnical Engineering*, Vancouver, BC.

Robertson, P.K. (2021). "Evaluation of flow liquefaction and liquefied strength using the cone penetration test: an update." *Canadian Geotechnical Journal*. <<https://doi.org/10.1139/cgj-2020-0657>>



---

Robertson, P.K., and Fear, C.E. (1995). "Liquefaction of sands and its evaluation." Keynote lecture. *Proceedings of IS Tokyo '95, the First International Conference on Earthquake Geotechnical Engineering*, Edited by K. Ishihara, A.A. Balkema, Rotterdam.

Robertson, P.K., de Melo, L., Williams, D.J., and Wilson, G.W. (2019). "Report of the expert panel on the technical causes of the failure of Feijao Dam 1." <<http://www.b1technicalinvestigation.com>>

Sadrekarimi, A., and Olson, S.M. (2011). "Yield strength ratios, critical strength ratios, and brittleness of sandy soils from laboratory tests." *Canadian Geotechnical Journal*, 48(3), 493–510.

Sasitharan, S., Robertson, P.K., Sego, D.C. and Morgenstern, N.R. (1993). "Collapse behavior of sand." *Canadian Geotechnical Journal*, 30, 569-577.

Schnaid, F., Bedin, J., Viana da Fonseca, A.J.P., and Moura Costa Filho, L. (2013). "Stiffness and strength governing the static liquefaction of tailings." *Journal of Geotechnical and Geoenvironmental Engineering*, ASCE.

Sotil, A., Soto, V., and Brouwer, K. (2020). "Reducing long term risk at the Candelaria tailings storage facility." *Proceedings of the 2020 Tailings and Mine Waste Conference*.

Verdugo, R., and Ishihara, K. (1996). "The steady state of sandy soils." *Soils and Foundation, Japanese Geotechnical Society*, 3(2), 81–91.

Vesic, A.S., and Clough, G.W. (1968). "Behaviour of granular materials under high stresses." *J. Soil Mech. and Found. Div.*, ASCE, 94(3), 661–688.



INTERNATIONAL JOURNAL OF  
**GEOENGINEERING  
CASE HISTORIES**

*The Journal's Open Access Mission is  
generously supported by the following Organizations:*



Geosyntec  
consultants

engineers | scientists | innovators

**CONE**TEC



**ENGEO**  
Expect Excellence

Access the content of the ISSMGE International Journal of Geoengineering Case Histories at:  
<https://www.geocasehistoriesjournal.org>